Original Research *Featured Article*

A human liver microphysiology platform for investigating physiology, drug safety, and disease models

Lawrence A Vernetti[1,2], Nina Senutovitch[1,2], Robert Boltz[1,2], Richard DeBiasio[1], Tong Ying Shun[1], Albert Gough[1,2] and D Lansing Taylor[1,2]

[1]University of Pittsburgh Drug Discovery Institute, University of Pittsburgh, Pittsburgh, PA 15260, USA; [2]University of Pittsburgh Dept. of Computational & Systems Biology, University of Pittsburgh, Pittsburgh, PA 15260, USA
Corresponding author: Lawrence Vernetti. Email: vernetti@pitt.edu
The authors Vernetti and Senutovitch have both contributed equally to submitted work.

Abstract

This paper describes the development and characterization of a microphysiology platform for drug safety and efficacy in liver models of disease that includes a human, 3D, microfluidic, four-cell, sequentially layered, self-assembly liver model (SQL-SAL); fluorescent protein biosensors for mechanistic readouts; as well as a microphysiology system database (MPS-Db) to manage, analyze, and model data. The goal of our approach is to create the simplest design in terms of cells, matrix materials, and microfluidic device parameters that will support a physiologically relevant liver model that is robust and reproducible for at least 28 days for stand-alone liver studies and microfluidic integration with other organs-on-chips. The current SQL-SAL uses primary human hepatocytes along with human endothelial (EA.hy926), immune (U937) and stellate (LX-2) cells in physiological ratios and is viable for at least 28 days under continuous flow. Approximately, 20% of primary hepatocytes and/or stellate cells contain fluorescent protein biosensors (called sentinel cells) to measure apoptosis, reactive oxygen species (ROS) and/or cell location by high content analysis (HCA). In addition, drugs, drug metabolites, albumin, urea and lactate dehydrogenase (LDH) are monitored in the efflux media. Exposure to 180 μM troglitazone or 210 μM nimesulide produced acute toxicity within 2–4 days, whereas 28 μM troglitazone produced a gradual and much delayed toxic response over 21 days, concordant with known mechanisms of toxicity, while 600 μM caffeine had no effect. Immune-mediated toxicity was demonstrated with trovafloxacin with lipopolysaccharide (LPS), but not levofloxacin with LPS. The SQL-SAL exhibited early fibrotic activation in response to 30 nM methotrexate, indicated by increased stellate cell migration, expression of alpha-smooth muscle actin and collagen, type 1, alpha 2. Data collected from the *in vitro* model can be integrated into a database with access to related chemical, bioactivity, preclinical and clinical information uploaded from external databases for constructing predictive models.

Keywords: *In vitro* liver model, hepatotoxicity, high content analysis, microphysiology systems, microfluidics, liver disease models

***Experimental Biology and Medicine* 2016; 241: 101–114. DOI: 10.1177/1535370215592121**

Introduction

Drug-induced liver injury (DILI), poor pharmacokinetic (PK) properties, as well as limited efficacy have historically been common causes for termination of compounds early in clinical trials. The poor concordance between animal testing and clinical hepatotoxicity is also well known.[1] In the past two decades, the pharmaceutical industry has applied 2D phenotypic and molecular-based *in vitro* assays, broad spectrum proteomics, metabolomics and toxicogenomics screening to address the challenge. These *in vitro* approaches were expected to lessen reliance on animal models by providing predictions of toxic liabilities, as well as serving as models for disease. However, these early approaches have only had limited success as predictive tools, but have been useful in early, high throughput, safety profiling and as tools to understand mechanisms of toxicity (MOT).[2]

There are now two major drivers for creating better human, *in vitro* models of hepatotoxicity and liver diseases that address the ''fit for purpose'' criteria used in the pharmaceutical industry: (1) high throughput, human, 2D and 3D, live, physiological liver models in the microplate format that can be used in early safety and efficacy profiling of relatively large numbers of compounds; and (2) human, 3D, live, biomimetic, microfluidic models that exhibit the

ISSN: 1535-3702

physiological impact of continuous flow on organ functions; long-term (at least 28 days) functioning for modeling diseases and characterizing chronic toxicity; as well as compatibility for microfluidic coupling, with proper scaling, of multiple organs-on-chips, such as a gut, liver, and kidney, to model partial human functions such as ADME-TOX.[2–5] In addition, the microfluidic devices can be used to test more challenging MOT, as well as complex disease models studied over an extended period of time where flow is critical.[6–8]

For the high throughput fit for purpose driver, simple cytotoxicity assays have historically been used to assess potential risk. Commonly used cytotoxicity indicators include LDH leakage, live/dead dyes such as Neutral Red, MTT, fluorescent dyes such as 5-Chloromethylfluorescein Diacetate (CMFDA) or Calcein AM and intracellular ATP.[9] Although simple cytotoxicity assays are often used to rank order compounds by overall toxicity risk and to eliminate highly toxic compounds, the assays can have higher levels of false positive and negative rates when compared to multiplexed analysis, which has limited their acceptance as stand-alone criteria for selecting candidate compounds.[10–12] The combined use of primary hepatocytes, MOT measurements and estimations of total exposure have proven moderately successful for predicting human hepatotoxicity.[12,13] However, it is clear that ''silent'' toxic agents still pass through these profiles while some safe candidate compounds might be eliminated before additional animal testing.[12,14–17] Recently, there has been significant progress in creating human, live, 3D models of the liver in the microplate format that should serve the higher throughput and physiological relevance criteria.[6,7] It is expected that these models will continue to evolve in performance.

A valuable human, 3D, live, biomimetic, microfluidic model requires the combination of: a biologically relevant matrix material to support a 3D multicellular human microenvironment; all cell types required for organ functionality, media formulations to provide specific organ nutritional and hormonal needs; flow through media to provide the physiologically relevant flow stimulation, drug exposure, sample oxygenation, replenishment of nutrients, and removal of waste products to improve the performance of the model; and a device design that is robust, reproducible, and is expected to be cost- and time-effective when compared with animal testing. When combined with real-time mechanistic readouts, such models are expected to exhibit improved responsiveness to toxic agents and disease processes. Approaches that combine these elements are described as microphysiological systems, ''organs-on-a-chip'' or organoids.[18,19]

This paper reports on the construction of a first generation design for a human, 3D, four-cell, microfluidic model of the liver in a microfluidic device that addresses most of the optimal characteristics of a microphysiological system (Table 1). Figure 1 places this model in the context of a platform that integrates multiple data types to ultimately enable predictive modeling. This liver model is constructed using three human, non-parenchymal cell lines (NPCs) and a single lot of cryopreserved human parenchymal hepatocytes. The results indicate that the sequentially layered cells ''self-assemble'' into a layered tissue-like architecture with many of the organizational and functional features of the liver sinusoidal unit. A portion of the cells in the SQL-SAL are transduced with fluorescent protein biosensors that are incorporated into the genome of the hepatocytes and NPCs, here referred to as sentinel cells. The biosensors in the microfluidic device allow capture of real-time, functional readouts with a confocal high content analysis (HCA) imaging system. The SQL-SAL maintains stable liver function for up to one month and is used here to demonstrate acute and sub-chronic liver injury including direct induction of apoptosis, induction of apoptosis by immune-mediated toxicity, and an early indication of the activation of a fibrosis response. The combination of live cell monitoring of physiological processes, a database to manage, analyze, and model the data, as well as direct access to related chemical, bioactivity, preclinical, and clinical information from external databases, provides an integrated microphysiological platform for assessing human toxic liabilities, as well as efficacy of experimental compounds for liver diseases. This is the first step in creating an optimal platform for stand-alone liver toxicity and disease modelling, as well as coupling with other organs-on-chips. Table 1 also addresses the planned evolution of the platform.

Materials and methods

Cell sources

A selected lot of cryopreserved primary human hepatocytes found to have >90% viability and re-plating efficiency post thaw, was obtained from Life Technologies (Grand Island, NY, USA). EA.hy926 human umbilical vein cell line and U937 human histocytic lymphoma (human monocyte) cells were obtained from ATCC (Manassas, VA, USA). LX-2 human stellate cells were generously provided by Martin Yarmush, Mass General Hospital and are also available from EMD Millipore (Billerica, MA, USA). The EA.hy926cell is a fusion product of the HUVEC and A549 cells. EA.hy926 cells release monocyte chemoattractant protein 1 (MCP) in response to inflammation and do not require the use of growth modulators (e.g. VEGF to support HUVECs).[20] PMA treatment will differentiate U937 cells into mature macrophages which release various cytokines and chemokines in response to soluble stimuli. In particular, differentiated U937 macrophages release human tumor necrosis factor alpha (TNFα) and IL-6 in response to LPS treatment, a condition reported to induce the immune mediated liver toxic response *in vitro* and *in vivo* models.[7,21] The LX-2 cell is an immortalized human hepatic stellate cell that constitutively expresses key receptors regulating hepatic fibrosis and proliferate in response to PDGF, a prominent mitogen contributing to liver fibrosis.[22,23]

Liver model assembly

A single chamber commercial microfluidic device (TEMS single channel device, SCD-47, Nortis, Inc. Seattle, WA, USA)[24] was selected for optical quality for imaging and robust mechanical design. The devices were stored in PBS until use. The interior of the devices was rinsed in absolute

Table 1 Optimal characteristics of a human, liver-on-a-chip platform

Optimal Characteristics	Characteristics of Present SQL-SAL
Robust – data are reproducible from device-to-device and from day-to-day	Partial, chip-to-chip CV is $<30\%$, day-to-day CV is $<30\%$. Optimizing assays for small volumes to improve assay reproducibility
Easy to assemble and use – simple procedures lead to a high yield of functional models	Yes, $>90\%$ chips produce acceptable data
Biomimetic of major acinus toxicology and drug metabolism functions – e.g. **ROS, mitochondrial dysfunction, apoptosis, necrosis, Phases 1, 2, and 3 elimination, immune activation, fibrosis activation** macro- and micro-vesicular steatosis, phospholipidosis, and disease models	Yes, validated or demonstrated assays for bolded functions
Biomimetic of liver acinus structure – endothelial cell layer isolates hepatocytes from flow	Partial isolation of hepatocytes by endothelial cells. Next generation will improve the acinar structure by testing additional methods of cell layering, including bio-printing.
Includes continuous fluid flow – supplies nutrients, O_2 and removes waste products	Yes, flow rate is scaled to the scale of the model and supplies nutrients and removes waste. O_2 concentrations need to be characterized by integrated micro-clinical analyzer that is in development.
3D, multicellular system consisting of human liver acinar cells – Hepatocytes, endothelial, stellate and Kupffer cells	Yes, four relevant human cell types. Non-parenchymal cells (NPCs) are cell lines for simplicity. Next generation will test iPS-derived hepatocytes and at least primary human NPCs
Allows real-time transmitted light and fluorescence imaging – transparent top and bottom made of low fluorescence materials	Yes, current materials allow transmitted light and have very low fluorescence interference. Future plastic devices will maintain optical quality
Minimal or no PDMS – materials are not adsorbent or absorbent to drug-like chemicals	Current generation contains some PDMS limiting use with some hydrophobic compounds, but next generation will use protein-coated plastic and low binding tubing material.
Includes vascularization	No. This is now in development
Ability to establish zonation – minimal media buffering to allow a gradient of pH and O_2 in device, model elongated along flow with dimensions that mimic an acinus	No. Next generation will be closer to acinus dimensions and support establishment of zonation
Device can be easily coupled to other devices – reliable and easy to use fluid connections, tubing with low adsorption that minimizes dead volume	Yes, current model has metal tubes for attaching flow lines, future models will use low volume connectors and tubing with low binding of hydrophobic compounds
Database to manage and analyze data – supports results from imaging, biochemistry and MS, and provides tools for modeling human PK/PD, toxicity and efficacy	Partial, current database support all three data sources and has capability for managing reference clinical trial and post-marketing data to support modeling

ethanol and dried under vacuum prior to protein coating with 100 μg/mL bovine fibronectin and 100 μg/mL rat tail collagen, type 1, alpha 2 in PBS as previously described.[25] Cryopreserved hepatocytes were thawed following the manufacturer recommendations. A portion was incubated 2 h in lentiviral supernatant generated from pCT-mito-GFP (apoptosis biosensor) or pLVX-IRES-puro-HyPer-dmito (hydrogen peroxide biosensor, supplemental materials). Hepatocytes were pelleted at 50 g × 3 min, resuspended at 2.5×10^6 hepatocytes/mL in Williams E medium supplemented with 5% fetal bovine serum (Cellgro, Manassas CA), 100 μg/mL Penicillin Streptomycin (HyClone, Logan, UT), and 2 mM L-glutamine and injected into the interstitial compartment of the device for overnight incubation at 37°C to allow adherence and spreading. A mixture of 2.0×10^6 EA.hy926 cells/mL and 1.6×10^6 U937 monocytic cells/mL (see supplemental materials for details of cell characterization and differentiation) in DMEM (Gibco, 10% FBS, 1 × penicillin/streptomycin) was then injected on top of the attached hepatocytes, incubated for 2 h at 37°C before the final injection of 0.2×10^6 LX-2 cells suspended in 1 mL of a 2.5 mg/mL solution of pH 7.2 rat tail collagen/10 mM HEPES/HBSS. The devices were inverted for 1 h at 37°C during collagen polymerization to ensure an initial spatial separation of hepatocytes and stellate cells. The devices were re-inverted to their normal orientation and incubated overnight to allow stabilization of the model before initiating 5 μL/h perfusion with hepatocyte maintenance media (HMM, Life Technology, Grand Island, NY, USA) supplemented with 100 nM dexamethasone at 37°C in 5% CO_2. The density of each cell type and perfusion rate was determined by use of allometric scaling as presented in Table 2. Determination of flow characteristics in the devices using fluorescent tagged dextran particles is presented in the supplemental materials (Figure S1, Supplementary material). Z-plane images in SQL-SAL devices containing biosensor expressing hepatocytes, stellates, and endothelial cells were collected by confocal HCA imaging to construct a spatial model of the distribution of cells on Day 0 and Day 7. Images were collected starting 200 μm above the attachment surface and serial sectioning down every 10 μm from 200 to 0 μm.

Device testing

Troglitazone, nimesulide, caffeine, trovafloxacin, levofloxacin, LPS and methotrexate (all from Sigma, St Louis, Mo) were administered into the devices as 1% DMSO solutions

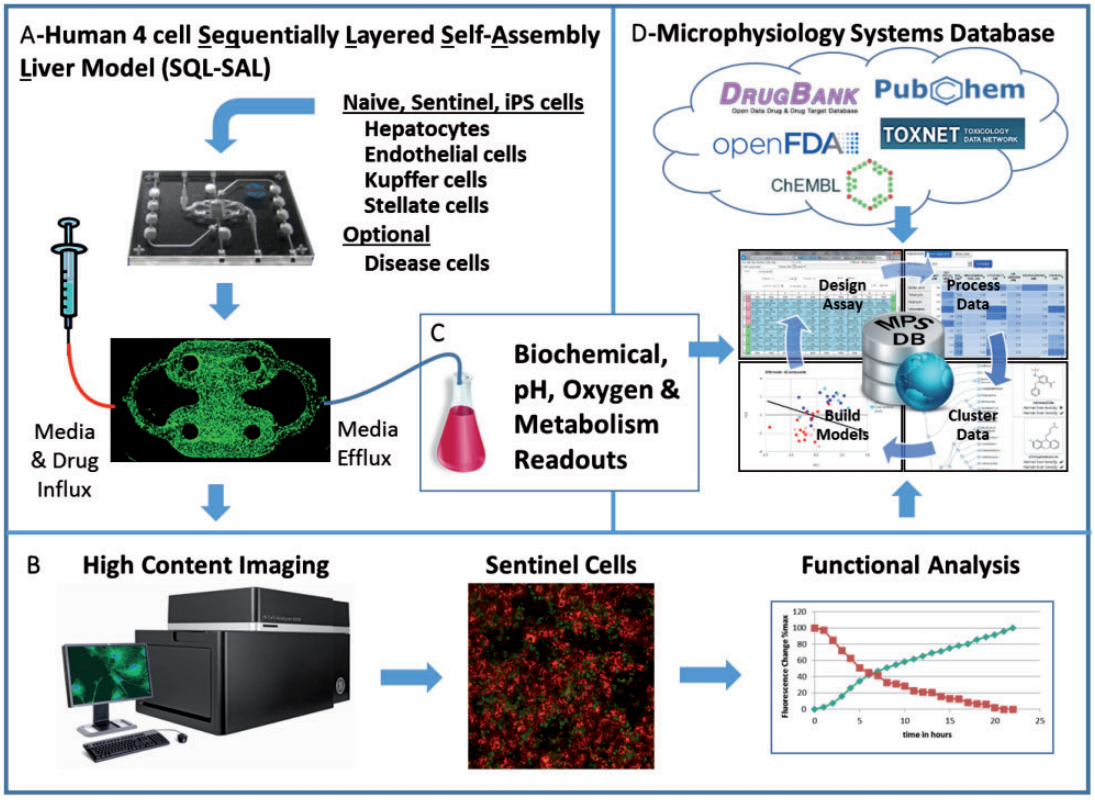

Figure 1 Overview of the Human Liver Microphysiology Platform (HLMP) for studying human organ physiology, disease models and drug safety testing, including coupled, multi-organ modules. The HLMP is comprised of: (a) the Human, 4-cell Sequentially Layered Self-Assembly Liver Model (SQL-SAL) constructed from a microfluidic device and a minimum of four human cell types, a fraction of which are ''sentinel'' cells expressing fluorescent protein biosensors, optionally including disease-specific cells such as cancer cells and iPS-derived cells. Data are collected from the model via (b) high content imaging readouts of transmitted light and/or fluorescence, an example of which shows hepatocyte sentinel cells expressing an ROS biosensor in green and TMRE labeling for mitochondrial membrane potential in red. Data are also collected (c) from biochemical and mass spectrometry readouts and will include media pH and media oxygen content in the future. (d) The Microphysiology Systems Database (MPS-Db) accesses chemical and bioactivity data for test compounds from external databases; while multiplexed organ model data is uploaded from the SQL-SALA outputs for data management, association with external data sources, as part of the analysis and to build predictive models of human efficacy and toxicity

Table 2 Allometric scaling of SQL-SAL model

Scaling feature	Human	μHuman	SQL-SAL Model 0.3 μHuman	Ref.
Flow Rate (μL/min)	230,000–800,000	0.23–0.8	0.083	68
Mass (g)	1500	0.0039	0.001	67
Hepatocyte density (cells/g)	1.39E + 8	1.39E + 8	1.39E + 8	67
Cell type	**Cell count (percent)**	**Cell count (percent)**	**Cell count (percent)**	
Hepatocyte	15.6E + 10 (60%)	406,575 (60%)	125,000 (56%)	67
Endothelial	5.21E + 10 (20%)	135,525 (20%)	50,000 (22%)	67
Kupffer	3.91E + 10 (15%)	101,644 (15%)	40,000 (18%)	67
Stellate	1.30E + 10 (5%)	33,881 (5%)	10,000 (4%)	67

in HMM at the final concentrations. To achieve testing of up to the recommended 100 × C_{max} for *in vitro* liver systems,[26] 1.0% DMSO final concentration was used to improve compound solubility. 1.0% DMSO is on the high end of published concentrations,[7,27–29] but the negative control, caffeine in 1.0% DMSO as well as DMSO alone, had no impact on the parameters measured in the devices. The flow was temporarily halted to allow imaging of each device using the GE IN Cell 6000 (GE LifeSciences, Piscataway NJ, USA) equipped with an environmental chamber to maintain 37°C and 5% CO_2 (see below, HCA imaging and analysis). Flow was re-established in the devices after image collection.

Image and efflux media collection

Drug exposure by perfusion was initiated (day 0) following the two days to assemble and stabilize the model. Images

were collected at initiation of drug exposure (day 0, time 0), and again at 3 h, 24 h, then every third day up to day 10 for immune-mediated studies, day 21 for fibrosis activation studies or day 28 for toxicity studies. Secreted media was collected daily and analyzed for LDH leakage on days 0, 1, 2, 3, and 4 and then approximately every other day up to day 21 or 28. Albumin and urea synthesis were measured from daily media secretions collected from control liver devices on days 0, 1, 3, 10, 13, 17, and 25 and from drug-treated devices on days 1, 3, 10, 17, and day 21 or 28.

Efflux media collection and biochemical measurements

Albumin was measured using an enzyme linked immunosorbent assay (Bethyl Laboratories, Montgomery, TX, USA). LDH (CytoTox 96, Promega, Madison, WI, USA) and urea nitrogen (Urea Nitrogen Test, Stanbio Laboratory) was measured using colorimetric assays. Human TNF-α chemiluminescent ELISA was performed as described by manufacturer guidelines (ThermoFisher, Pittsburgh, PA, USA). All biochemical assays performed on the efflux media were performed in 384 well microplates according to manufacturer's instructions with the exception of the blood urea nitrogen (BUN) assay, which was modified from the manufacturer's protocol by reconfiguring for a 384 well microtiter plate and increasing the incubation of reactants from 60 to 90 min at 60°C before reading. All biochemical assays were conducted on 10 μL of media for each readout and measured on a SpectraMax M2 (Molecular Devices, Sunnyvale, CA, USA) microtiter plate reader. All sample results were calculated by interpolation of sample values from standard curves performed in parallel.

Drug metabolism measurements

Hepatocyte maintenance media supplemented with 5 μM testosterone, 10 μM diclofenac or 10 μM phenolphthalein, and 10 μM 7-ethoxyresorufin (EROD) were perfused through two or more test devices on days 10–12, 14, or 23, respectively. The efflux media was collected over a 24-h period. The drug metabolites were extracted from collected efflux media (Supplementary material) and measured using a Waters Acquity UPLC (Milford, MA, USA) using a C18, 1.7 μm, 2.1 × 100 mm reversed-phase column. Separation was carried out in an acetonitrile:water (0.1% formic acid) gradient using conditions presented in Table S1, Supplementary material. Detection of the metabolite peak was achieved in the positive ion mode with a TSQ Quantum Ultra Mass Spectrometer (ThermoFisher, Pittsburgh, PA, USA), interfaced via an electrospray ionization (ESI) probe (Supplementary material). The metabolite from EROD was measured directly in efflux media on a fluorescent spectrophotometer, as described in the Supplementary material.

Bile efflux testing

Hepatocytes in control devices were tested for normal canalicular efflux of CMFDA at days 10 and 21. Troglitazone inhibition of canaliculi efflux was demonstrated with day 10 devices. Briefly, the devices were perfused with HMM containing either vehicle (1% DMSO) or 50 μM troglitazone for 30 min. CMFDA (Life Technologies, Grand Island, NY) was prepared at 1 μM in HMM and added as a bolus into the assembled device. The devices were removed from perfusion apparatus and placed on the IN Cell 6000 HCA instrument for collection of 488/525 nm (ex/em) images at 10-min intervals over 1 h.

HCA imaging and analysis

All images were collected with a 10× or 20× objective using the IN Cell 6000 in confocal mode detailed in Supplementary material. The protocol was configured to collect images at 488/525 nm (ex/em, green channel) and/or 561/605 nm (ex/em, red channel) on 25 or 90 fields with a 10 × (0.45 N.A) or 20 × (0.45 N.A.) objective, respectively. These protocols imaged the entire cell attachment surface area. The images collected from the central region of the chamber were used for analysis (10 images at 20×and 27 images at 10×, Figure 2(b)).The aperture slits were set to 1.47 and 0.85 Airy units for the 10× and 20× objectives, respectively. The apoptosis biosensor (Supplementary material) in hepatocytes was imaged in the green channel and analyzed using two different application methods in MetaXpress 4 software (Molecular Devices, Sunnyvale, CA, USA). (a) The multi- wavelength cell scoring application module was used to quantify changes in cell average fluorescence intensity as the indicator of apoptosis; and (b) the integrated morphometric module was used to quantify changes in cellular area of hepatocytes expressing the apoptosis biosensor. The ROS biosensor was measured as the time-dependent increase in cellular intensity at 488/525 nm (ex/em) reflecting the increase in ROS. Additional imaging processing details are provided in the Supplementary material. Details on the development and quantitation of biosensors in sentinel cells will be published elsewhere.

Indirect immunofluorescence labeling and quantitation

Relative protein expression of human alpha- smooth muscle actin (alpha-SMA) and collagen type 1, alpha 2 (COL1A2) protein in LX-2 cells transduced with pLVX-IRES-mito-mKate2 biosensor (to identify the cells) was quantified on day 21 in paraformaldehyde fixed devices using standard indirect immunofluorescence methods (Supplementary material). The expression of alpha-SMA or COL1A2 protein was quantified as the ratio of the average cellular intensity of the respective antibody label in the stellate to the non-stellate cell population using Fiji (ImageJ, Supplementary material).

Statistics

Differences in drug and control population measurements reported as ''significant'' have a $p \leq 0.05$, as determined by application of a *t*-test with the assumption of equal variance.

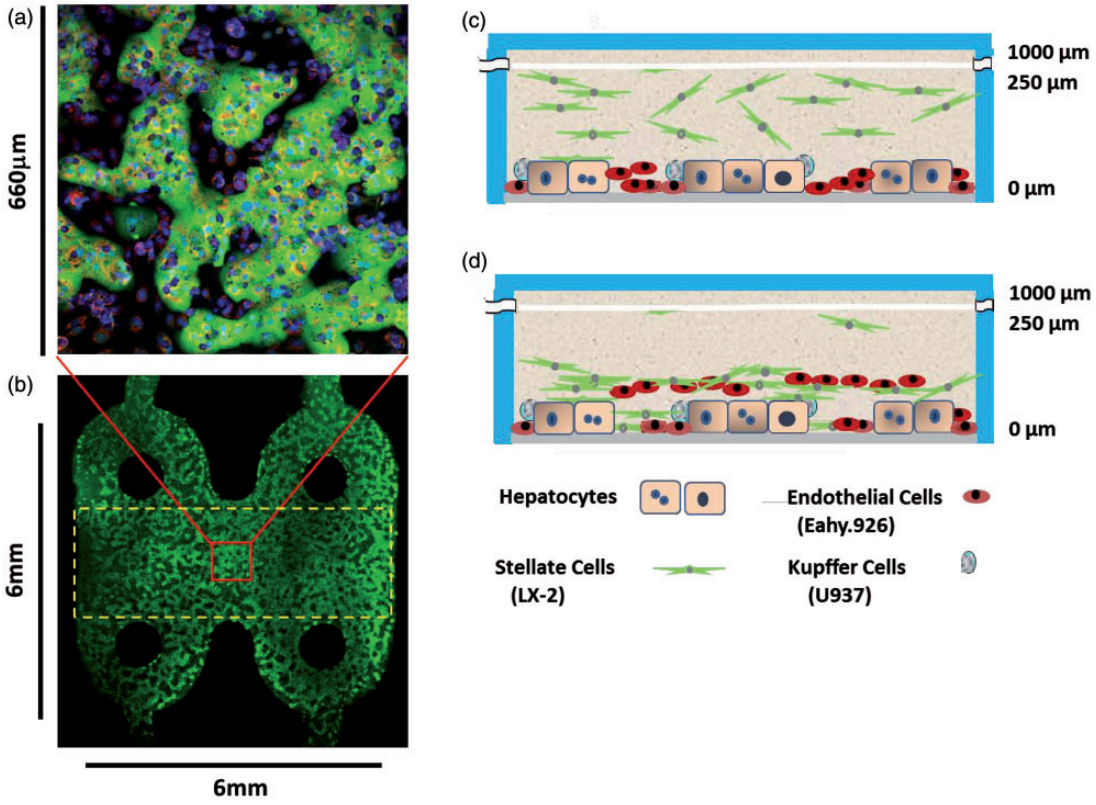

Figure 2 Cellular organization in the SQL-SAL. (a) Image of the organization of cells in the SQL-SAL. Primary hepatocytes self-organized into cords by day 7 (CMFDA labeling to highlight hepatocyte cords). The other cell types are sequentially layered in the device and self-assemble relative to the hepatocytes. Mitochondria are labelled with TMRE (red) and cell nuclei with Hoechst (blue). (b) Image montage of SQL-SAL device with labeled hepatocytes in cords (CMFDA, green to identify the hepatocytes). The cells are under constant flow at ca. 5 µL/h with the influx port at the top and the efflux at the bottom. The red box represents the relative size of a 20× field within the chamber shown in A and the dashed yellow box shows the region from which image fields were analyzed. Approximately 225,000 total cells are present in the entire chamber, added in physiological ratios of hepatocytes and non-parenchymal cells to create a ca. 0.3 micro-human. (c) Cross-section diagram based on confocal images of the typical cell organization in SQL-SAL on day 1 after cell seeding. Hepatocytes are first seeded on a layer of collagen. Endothelial cells (EA.hy926) and Kupffer-like immune cells (U937) are seeded 18–24 h after hepatocytes and initially localize with the hepatocytes. LX-2 stellates are seeded last, evenly dispersed in the collagen layer. (D) Diagram of typical cell organization in the SQL-SAL model 7 days after cell seeding, when endothelial cells and stellate cells are found in a layer above the hepatocytes, as well as some localized between hepatocytes. The cells in the diagrams C and D were quantified from serial confocal scans taken 10 µm apart starting from the hepatocyte layer

Results

Structure, long-term health, and normal function

The uniformity of media perfusion throughout the entire model was evaluated by time-lapse imaging of a bolus injection of fluorescent dextran (10 kD), which indicated consistent media exchange across and through the chamber (Supplementary material, Figure S1). The cellular organization and formation of hepatic cords by day 7 in the SQL-SAL were defined by confocal HCA (Figure 2(a) and (b)). Transmigration and reorganization of endothelial and stellate cells into a layered tissue proximal to the cords was quantified by counting fluorescent protein biosensor labeled cells in 3D image stacks acquired on day 7 (diagrammed in Figure 2(c) and (d)). A partial sinusoidal structure was attained by Day 7.

LDH leakage was stable in the devices during the 4-week incubation period, following an initial decrease in the efflux media levels on days 0–2 (Figure 3a). Albumin production was retained at a stable level during the ca. one month long testing (Figure 3b) and was consistently higher than in static culture (Figure 3b) as previously reported.[30,31] In addition, the rates of albumin production in the SQL-SAL model were found to be comparable to previously published reports.[7] Urea synthesis was found to be comparable to some published findings but lower compared to other published findings.[7,32] In addition, we found urea synthesis declined by day 25. Expression of the cytochrome C apoptosis biosensor increased from day 0 to 10, then stabilized for at least 28 days (Supplementary material, Figure S2).

The LC MS/MS was used to identify 6-β hydroxytestosterone (Cyp 3A4 testosterone metabolite), phenolphthalein-glucuronide (phase 2 phenolphthalein conjugate), and 4-hydroxydiclofenac (Cyp 2C9 diclofenac metabolite) extracted from efflux media in SQL-SAL devices perfused on days 10, 12, and 14, respectively (Table 3). Resorufin, the fluorescent product driven by Cyp 1A1/2 metabolism of 7-ethoxyresorufin (EROD) was identified in the efflux media in a SQL-SAL device perfused on day 23 with 10 µM EROD (Table 3). The specific cytochrome P-450 isoenzyme or conjugation reaction is consistent with published findings.[33–38] The retention time, parent to daughter fragmentation product, and mass area under the curve for the metabolites are presented (Table 3). Only the identification

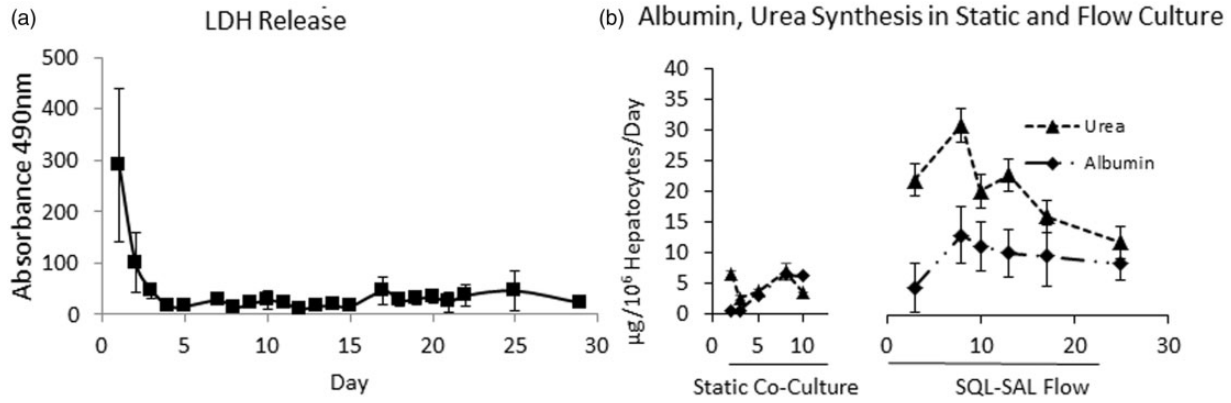

Figure 3 Long-term health and stability of hepatocytes in the SQL-SAL. (a) Lactate dehydrogenase (LDH) leakage measurements in efflux media are stable from day 3 to 28. (b) Albumin output in the efflux media is relatively stable and physiological for at least 25 days and is elevated relative to that measured in static co-cultures. Although urea output is stable for at least 21 days and elevated relative to static co-cultures, it is lower than most published levels and declines by day 25. Results presented as mean ± SD from 3 (days 3, 10, and 17) or 4 devices (days 7, 13, and 25) or three transwells

Table 3 Identification of specific Phase 1 and Phase 2 drug metabolites

Test compound concentration	Metabolite	MRT*	PDT†	Metabolite found in efflux media (AUC)	Cyp, Conjugation Enzyme	Ref.
5 μM Testosterone	6β-hydroxytestosterone	2.7	305 → 269	27921 ± 19523*	Cyp 3A4	33,69
10 μM Diclofenac	4′-Hydroxydiclofenac	3.1	312 → 231	36943 ± 28302†	Cyp 2C9	70,71
10 μM Phenolphthalein	Phenolphthalein glucuronide	2.5	495 → 319	231852 ± 94227†	UDP-glucuronyltransferase	32
Test compound concentration	**Metabolite**	**Pmol resorufin influx media**		**Pmol resorufin efflux media**	**Cyp**	**Ref.**
10 μM EROD‡ (7-ethoxyresorufin)	Resorufin[3]	0		22 ± 16§	Cyp 1A1/2	34,35

Metabolite retention time (MRT); Parent to daughter ion transition (PDT).
*Values represent the mean mass area under the curve ± SD; $n = 4$
†Values represent the mean mass area under the curve ± SD; $n = 2$
‡EROD non-fluorescent; resorufin measured at 530/590 nm (ex/em).
§Values represent the mean ± SD; $n = 2$.

of the metabolite is reported, as the quantitative analysis of drug and metabolite is limited by the presence of PDMS, a material known to adsorb some hydrophobic compounds.[39]

Toxicity testing

The literature on lentiviral transduction with reasonable expression levels indicates that cellular functions are not impacted[40–43] and we found no differences in the measured responses of HepG2 cells, transduced and non-transduced under treatment conditions that induced oxidative stress (unpublished data). Overt cytotoxicity, measured as LDH release from the SQL-SAL under continuous perfusion, was found on day 4 at 180 μM ($30 \times C_{max}$) troglitazone and delayed until day 13 at 28 μM ($4 \times C_{max}$) troglitazone compared to 600 μM ($100 \times C_{max}$) caffeine used as the negative control (Figure 4a). The higher troglitazone concentration resulted in a sharp decrease in albumin and urea starting at day 1 of treatment, which was distinct from a gradual decrease of albumin and urea with 28 μM troglitazone versus caffeine control (Figure 4(b) and (c)). Finally, the SQL-SAL demonstrated normal and troglitazone-inhibited bile efflux as measured by CMFDA dye uptake and secretion into canalicular spaces between hepatocytes (Figure 4(d) and Supplementary material, Figure S3).

The induction of apoptosis, as measured by loss in the intensity of the cytochrome C biosensor in the mitochondria in sentinel cells, began on day 1 and on day 10 in the liver devices that received 180 μM and 28 μM troglitazone, respectively (Figure 5a). The time-dependent loss of mitochondrial cytochrome C biosensor was evident in images acquired over time (Figure 5(b) and (c)). There was no appreciable effect of 600 μM caffeine on induction of the hepatocellular apoptosis biosensor over the four-week treatment (Figure 5a). Further characterization of troglitazone-induced hepatocellular apoptosis was performed using a mitochondrial-targeted ROS biosensor that indicated an increase in ROS when measured over 24 h (Figure 5d). Images from the real-time readout also demonstrated increased ROS biosensor fluorescence (Figure 5(e) and (f)). Then 210 μM nimesulide ($10 \times C_{max}$) was used as a second hepatotoxic drug and produced a rapid increase of

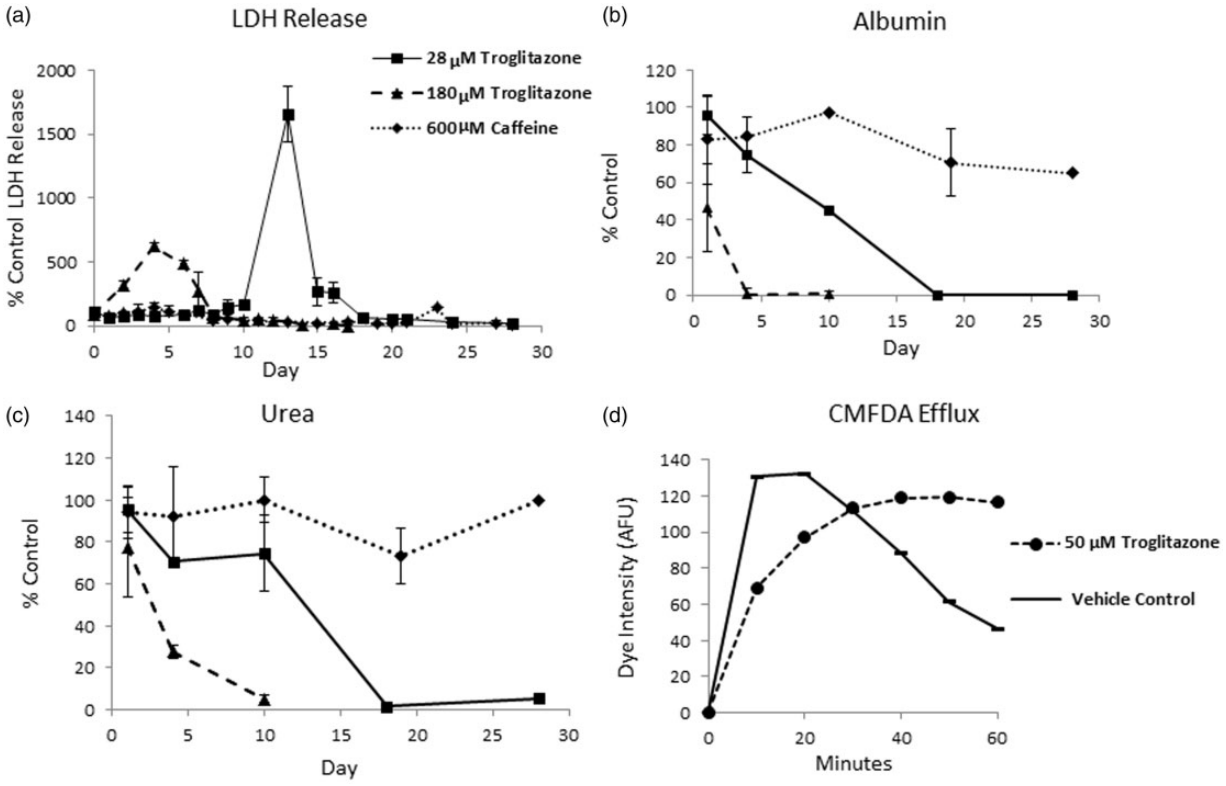

Figure 4 Troglitazone drug treatment demonstrates time- and dose-dependent toxicity. The SQL-SAL was exposed to troglitazone 28 μM ($4 \times C_{max}$), 180 μM ($30 \times C_{max}$), or caffeine 600 μM ($100 \times C_{max}$), as a negative control for 0–28 days. Note the figure legend is the same for figures a, b and c. (a) Troglitazone at 28 μM ($4 \times C_{max}$) induces significant levels of LDH release ($p \leq 0.05$) on days 13–15 with the peak loss occurring at~13 days and at 180 μM ($30 \times C_{max}$), and is significant ($p \leq 0.05$) on days 4–6 with a peak~4 days. (b) Troglitazone at 28 μM ($4 \times C_{max}$) induces a significant decline in albumin secretion ($p \leq 0.05$) on days 18–28 with the T½ on ~11 days and significant ($p \leq 0.05$) at 180 μM ($30 \times C_{max}$), on days 4–10 with the T½ on ~day 3. (c) Troglitazone at 28 μM ($4 \times C_{max}$) induces a significant decline in urea secretion ($p \leq 0.05$) on days 4–28 with the T½ of ~12 days and significant ($p \leq 0.05$) on days 4–10 with the T½ at ~ day 3 at 180 μM ($30 \times C_{max}$). Caffeine produced no significant effects from 0- to 28-day treatment in any measurement. (d) CMFDA fluorescence was monitored in hepatocytes at 10-min intervals for 60 min in a 10-day treatment with vehicle control (1% DMSO) or 50 μM troglitazone. Normal uptake and efflux of the dye is evident in vehicle control compared to the slower uptake and inhibition of efflux in a troglitazone-treated device (see Figure S4, Supplementary material). Values reported for (a)–(c) represent means and SD of replicate devices. *P*-values are calculated from drug treatments versus vehicle control data

apoptotic hepatocytes, with decreases in albumin, urea and a rapid release of LDH (Figure S4, Supplementary material).

To investigate immune-mediated hepatotoxicity in the SQL-SAL, differentiated U937 cells were used as surrogate Kupffer cells. The PMA differentiated immune cells released TNF-alpha in plate cultures in response to LPS exposure (Figure 6a). Drug challenge with 200 μM trovafloxacin ($40 \times C_{max}$) or 600 μM levofloxacin ($38 \times C_{max}$), with 1 μg/mL LPS, was used to investigate hepatotoxic response in a pro-inflammatory state. Increased LDH leakage was evident at day 3 in devices co-incubated with 200 μM trovafloxacin and LPS (trovafloxacin + LPS), but not in devices co-incubated with 600 μM levofloxacin and LPS (levofloxacin + LPS) (Figure 6b). A significant decrease in hepatocyte area (condensation) was measured as a potential real-time, read-out for hepatocellular injury. A positive correlation between trovafloxacin + LPS treatment and decrease in hepatocyte area with increased propidium iodide uptake was established from static transwell, four cell liver cultures (Figure S5, Supplementary material). A significant time-dependent decrease in hepatocyte cell area was measured after day 3 in 200 μM trovafloxacin + LPS indicative of apoptosis, while 600 μM levofloxacin + LPS did not induce apoptosis (Figure 6c). Interestingly, Levofloxacin + LPS exhibited an increase in hepatocyte area indicating that some impact on the hepatocytes other than apoptosis occurred. This observation will be followed up with more experiments in the future. Taken together, these findings are in agreement with rodent inflammatory models that have been developed to mimic human findings[44,45]; however, this *in vitro* model is human and the changes can be analyzed dynamically.

Disease model application

To explore the potential application of the liver model to elucidate fibrotic disease, the immortalized human stellate cells (LX-2) transduced with a biosensor to enable the tracking of cell division and movements were monitored for 21 days by confocal HCA. Over this time, the stellate cells transmigrated from an initial uniform distribution throughout the space above the hepatocytes into open spaces between the hepatic cords and into a layer just above the hepatic cords (Figure 7a). Furthermore, when the stellate cells contacted the hepatocytes, there was an increase in

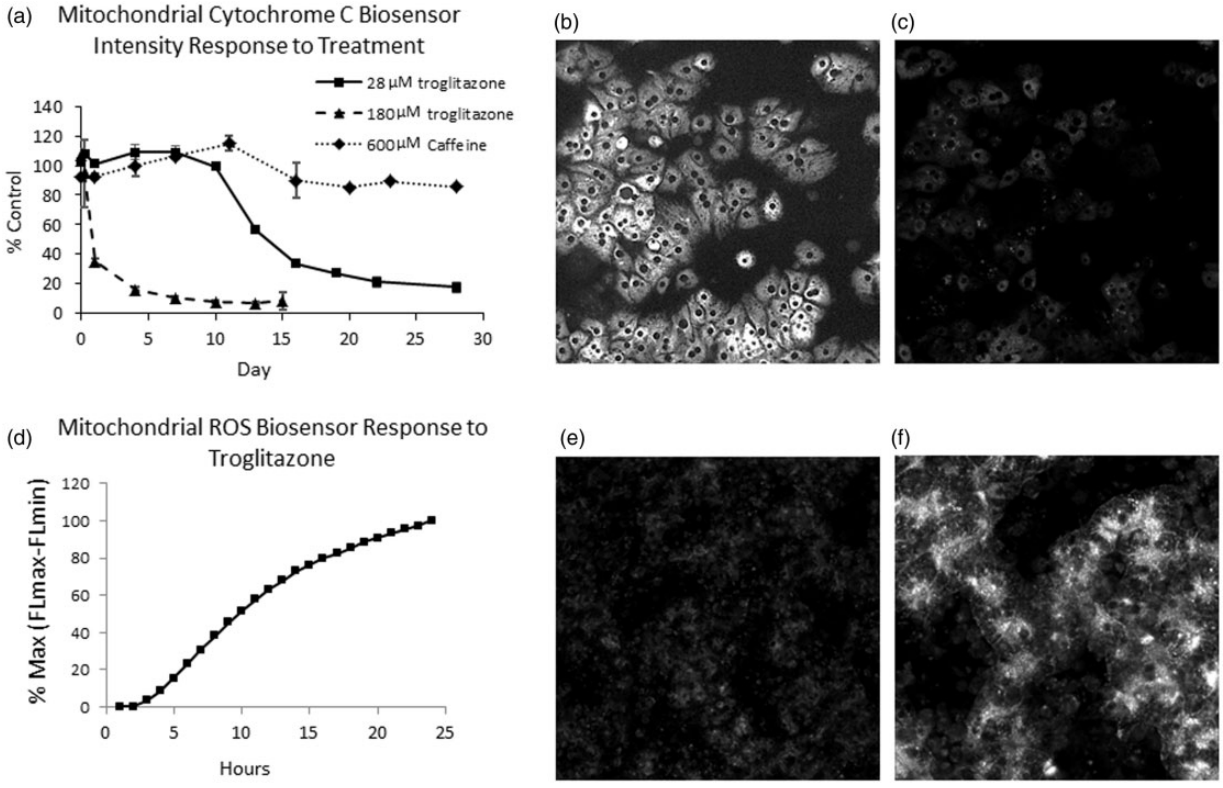

Figure 5 Live cell monitoring of hepatocellular fluorescent protein biosensors in sentinel cells that are mixed in with native cells demonstrate time and dose dependent toxicity. The SQL-SAL was exposed to troglitazone (28 or 180 μM), or caffeine (600 μM, negative control) for 0–28 days. (a) Troglitazone at 28 μM triggered significant levels ($p \leq 0.05$) of apoptosis in sentinel cells expressing the cytochrome C biosensor, on days 16–28 with the T½ at ~14 days and at 180 μM on days 1–15 with a T½ ~1 day. Caffeine treatment produced no significant effect over 28 days. Values represent the mean and error bars the SD of replicate devices. P-values are calculated for drug treatments versus vehicle control data. (b) An example of the bright, punctate, mitochondrial distribution of the cytochrome C biosensor in hepatocytes 2 h after treatment with troglitazone and (c) the loss of the cytochrome C biosensor signal from mitochondria with the fluorescence signal ''diluted'' in the cytoplasm following release evident after 14 h. (d) The activation of the ROS biosensor in hepatocytes treated with troglitazone is monitored using a 488 nm emission as a time-response curve from 0 to 24 h after validation of a ratio measurement (data not shown). (e) Minimal ROS signal is evident in sentinel hepatocytes at 4-h treatment. (f) Increase in intensity of the ROS biosensor is evident in hepatocytes at 19 h

the expression of human COL1A2 (Figure 7b). A hallmark of stellate cell transactivation from the vitamin A storage precursor into collagen depositing myofibroblasts is an increase in the expression of alpha-SMA.[46,47] Our results showed the stellate cells actively expressed increased levels of human COL1A2 and alpha-SMA in response to 30 nM methotrexate treatment over 21 days (maximum tolerated concentration of 100 nM determined in LX2 cultures; data not shown) (Figures 7(b) and 8).

Discussion

Although many *in vitro* models have been used to detect hepatotoxicity, pharmacokinetic properties and efficacy, none have yet successfully recapitulated the complex interactions between the different cell types, cell-to-cell signaling, flow within the liver, as well as oxygen and nutrient zonation (Table 1). Many of the *in vitro* models have proven capable of identifying the direct action of toxicants on the hepatocytes or have been found useful to identify the putative pathways and mechanisms of toxicity that have been linked to clinical hepatotoxicity, but they have had less success in predicting adverse clinical events or serving as models of liver diseases.[13,14,48] The work described herein demonstrates progress towards an improved physiological model system that will continue to evolve with increased functionality (Table 1). We have combined a very simple microfluidic device, 3 human, non-parenchymal cell lines together with primary human hepatocytes as the base-line cell system, a collagen matrix, a sequentially layered, self-assembly construct (SQL-SAL) and flow to create a robust and reproducible, generation one system with reasonable structure and functionality.

Despite the use of *in vitro* hepatotoxicity testing in the pharmaceutical industry to reduce the numbers of compounds with human toxic liabilities, DILI remains the leading cause of acute liver failure in the USA[49–51] and the field continues to rely on animal models of disease where the concordance with humans is low. Therefore, there has been a drive to construct more physiologically relevant, human, 3D ''organ'' models with various levels of complexity, including multiple liver cell types, longer-term viability, flow stimulation, and integrative analysis of multiplexed experimental data using computational models.[26,52–58] The human liver models have in common the goals to: retain important hepatocyte functions; extend culture time to

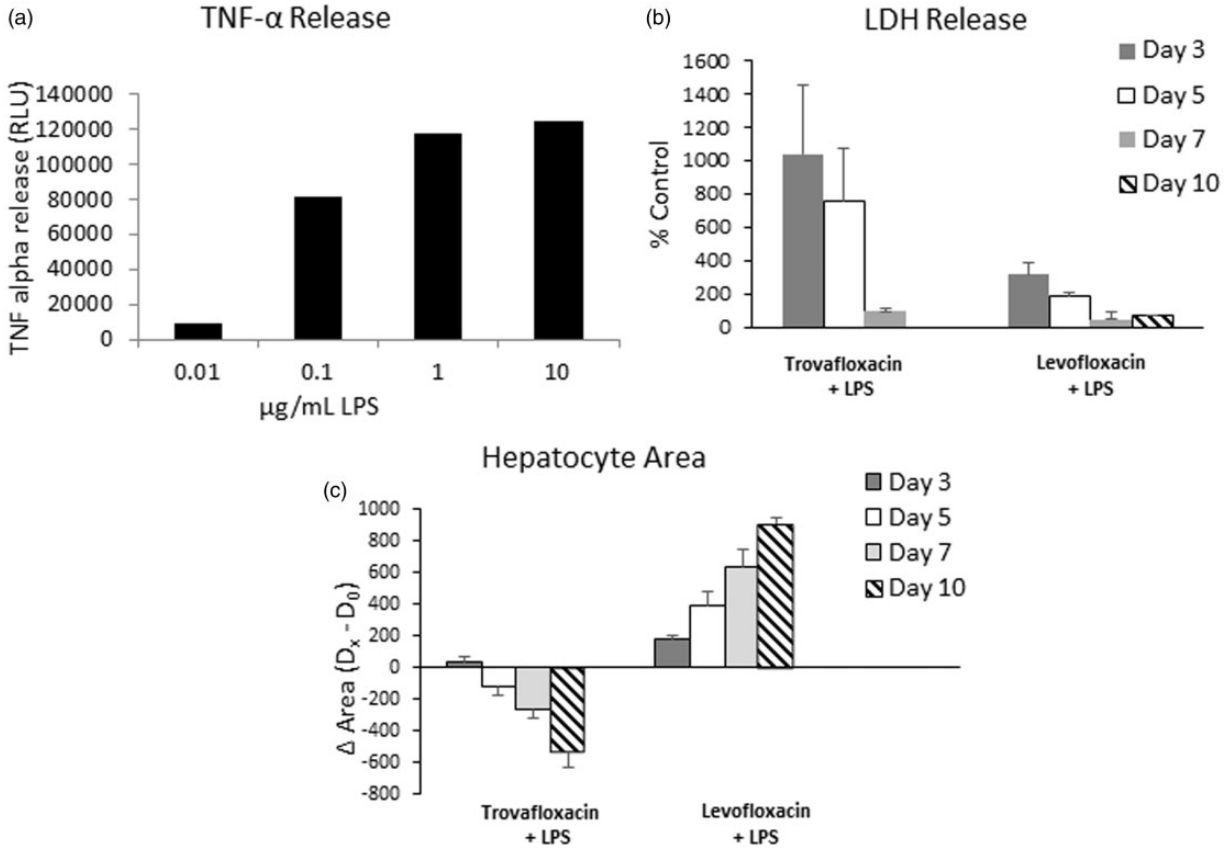

Figure 6 Demonstration of active immune function in the SQL-SAL. (a) Lipopolysaccharide (LPS) activated U937 cells release hepatotoxic TNF-alpha with an EC50 of 0.7 µg/ml in a static 96 well plate format. (B) Increased LDH leakage was evident in devices treated 3 and 5 days with 200 µM (40 × C_{max}) trovafloxacin co-incubated with 1 µg/mL LPS, but not with levofloxacin plus LPS. (c) The shift in toxicity is evident as a decrease in hepatocyte area measured in real time and achieved significance ($P \leq 0.05$) on days 3–10 in the SQL-SAL exposed to 200 µM trovafloxacin (40 × C_{max}) with 1 µg/mL LPS. The decrease in hepatocyte area with trovafloxacin co-incubated with LPS treatment was correlated with cell death measured by an increase in propidium iodide uptake (see Figure S6, Supplementary material). LDH and hepatocyte area results are the mean and SD of replicates per treatment group. *P*-values were calculated between devices treated with levofloxacin plus LPS and trovafloxacin with LPS. Although levofloxacin plus LPS does not induce apoptosis, it does cause an increase in the hepatocyte area. The biological basis for this change will be investigated in the future

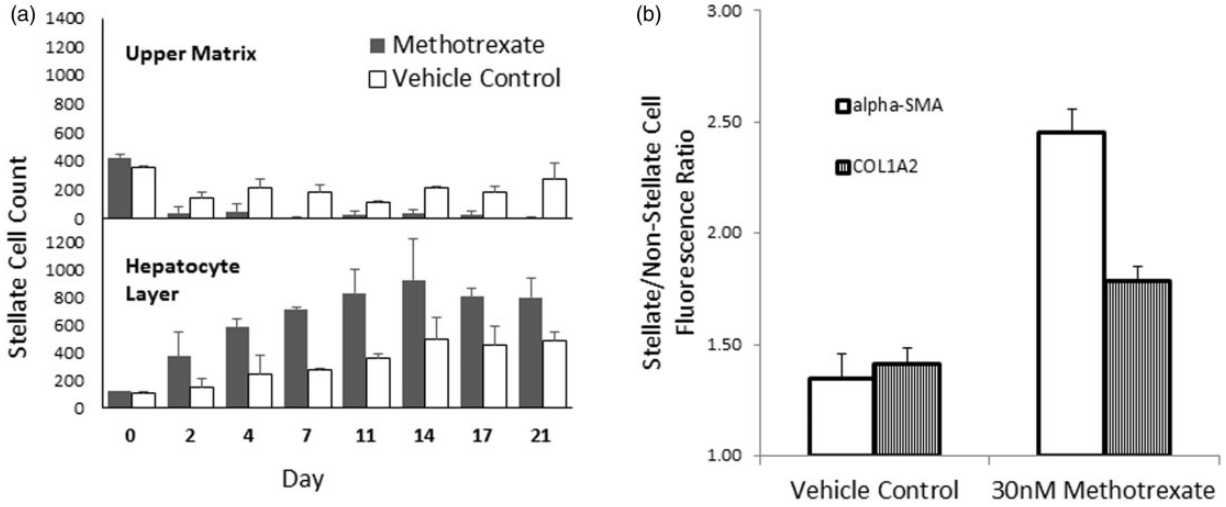

Figure 7 LX-2 stellate cell activation and migration in SQL-SAL. (a) In response to 30 nM methotrexate treatment over 21 days, LX-2 stellate cells transmigrate from the upper matrix and significantly accumulate ($p \leq 0.05$) proximal to the hepatocyte layer at an accelerated rate on days 4 and 7 and significantly decrease ($p \leq 0.05$) on days 7–17 in the upper matrix compared with vehicle control treatment. Values are the mean and SD of replicates. (b) Significant expression ($p \leq 0.05$) of human alpha-SMA (stellate cell activation marker) and collagen, type 1, alpha 2 proteins (COL1A2, marker for fibrosis) in LX-2 stellate cells on day 21, quantified by image analysis in paraformaldehyde-fixed and antibody-labeled SQL-SAL devices, is increased with 30 nM methotrexate treatment relative to vehicle control

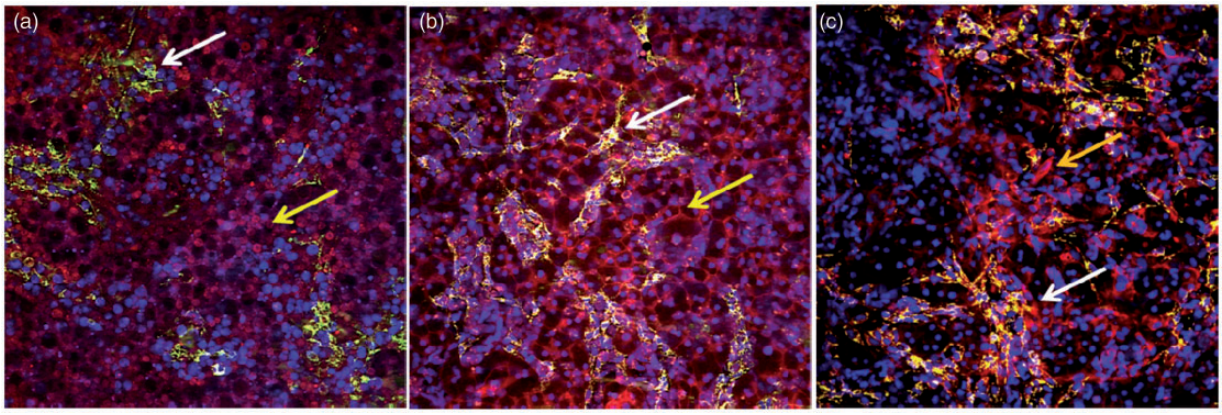

Figure 8 Representative images of LX-2 stellate cell activation that were quantified in Figure 8(b). (a) Immunofluorescence image of a SQL-SAL exposed to vehicle for 21 days, fixed and labeled with an anti-human alpha-SMA antibody. Minimal alpha-SMA expression (false colored red) is evident in green stellate cells (white arrow) or in hepatocytes (yellow arrow). (b) Immunofluorescence image of a SQL-SAL treated 21 days with 30 nM methotrexate, fixed and labeled with anti-human alpha-SMA antibody. An increase in alpha-SMA expression (false colored red) is evident by the in stellate cells (white arrow) and red color in hepatocytes (yellow arrow). (c) Immunofluorescence image of a SQL-SAL treated 21 days with 30 nM methotrexate, fixed and labeled with anti-human collagen 1A2 antibody. Expression of collagen is noted as increased yellow (white arrow) in stellate cells (false colored red). Not all stellate cells express collagen (orange arrow). Nuclei are false colored blue in all images

accommodate chronic exposure studies; incorporate non-hepatocyte cell components to study immune-mediated DILI, fibrosis or other diseases related to the liver; and to employ a variety of genomic, phenotypic, mass spectroscopy, cell biochemical and media secretion-based assays to evaluate liver health and function in response to challenges.[8,18,57] The ''fit for purpose'' criteria offers advantages to the scientific and regulatory community, given the examples of high throughput models with reasonable liver functions that have been used to test large numbers of compounds.[6,7,59] However, even more physiologically relevant platforms that include continuous flow and more read-outs, are important for more sophisticated investigations of human toxicity and liver disease progression, as well as multi-organ systems.

The present generation SQL-SAL can be maintained for at least 28 days under continuous media perfusion, demonstrated stable metabolic function, including phase 1 and phase 2 drug metabolism for 10–23 days (28-day studies are planned), polarized bile efflux, protein secretion, and responds predictably to known hepatotoxic compounds. The SQL-SAL can be used for the detection of early and specific modes of toxicity, such as apoptosis and ROS generation, via fluorescent protein biosensors. Monitoring drug toxicity and disease progression in a human, 3D, multiple cell-based platform when applied in parallel to the animal tests required before entering human clinical trials, is expected to improve predictions of human risk and drug efficacy. In time, these *in vitro* models are expected to reduce and ultimately replace animal testing.

An important advantage of the SQL-SAL is having a physiologically active liver model that can be treated and serially interrogated for damage induced by direct or indirect MOT and disease processes, for at least 28 days. For example, direct acting toxic agents such as troglitazone and nimesulide ultimately end in acute cellular necrosis or apoptosis, often as the result of metabolically reactive drug intermediates leading to dose- and time-dependent generation of oxidative stress, via mitochondrial dysfunction or interference with bile flow.[13] Indirect toxicity can be the result of an inflammatory response with cytokine release triggered by sub-acute hepatocyte damage by drugs such as trovafloxacin.[60] The release of cytokine mediators intensifies the hepatocellular injury, which, if not reversed, will ultimately leads to fatty liver or fibrosis and loss of liver function.[61]

More complex interactions between the cell types were demonstrated in the SQL-SAL by methotrexate-induced activation of alpha-SMA and COL1A2 positive stellate cells as an early indication of a fibrotic injury response. Although the progression and severity of the methotrexate fibrotic response reported from several clinical studies is conflicting, it is accepted that drug-damaged hepatocytes and immune cells can release molecular modulators that induce the differentiation of stellate cells into myofibroblasts which ultimately leads to hepatic fibrosis.[62–67] In addition, we found alpha-SMA expression was increased in hepatocytes under methotrexate treatment. Previous reports of alpha-SMA expression in hepatocytes resulting from the transition from epithelial to mesenchymal like morphology and mesenchymal marker expression have been inconsistent. Knock out studies in mice suggest that hepatocytes do not undergo the epithelial-mesenchymal transition (EMT) or express alpha-SMA during the fibrotic response.[68] However, recent evidence in the rodent supports the EMT in hepatocytes and the increased alpha-SMA expression.[69] In either case, the protein expression profile found in stellate cells in the SQL-SAL is consistent with the early activation of a fibrotic response. The extent and duration of the fibrotic response will be evaluated in more depth in follow-up studies.

The examples presented here for toxicity associated with troglitazone, nimesulide, trovafloxacin and methotrexate serve to describe the complexity of interactions between cell types and multifactorial initiating events in the development of liver injury or disease. The initial results in the

SQL-SAL demonstrate that differentiated cell and tissue-like functions are occurring in an interacting and interdependent physiological environment. At the present time, we are testing a number of known hepatotoxic and non-hepatotoxic compounds as well as paired sets of structurally related compounds of which one member of the pair exhibits hepatotoxicity while the other does not. These studies will be used to acquire a larger data set with which to build predictive models using our MPS-Db database (Figure S6, Supplementary material). A detailed characterization of the MPS-dB will be published elsewhere (Gough et. al., in preparation).

The SQL-SAL can detect early and specific modes of toxicity, e.g. apoptosis and ROS; with the use of fluorescent protein biosensors in ''sentinel'' cells with 3D, time series image analysis, an approach that highlights the value of integrated fluorescence biosensors in reporting mechanistic toxicity. Current efforts seek to characterize the use of a broader set of biosensors to determine additional clinically important modes of toxicity and liver disease progression.[70] We are also expanding the SQL-SAL for disease studies through the use of normal and diseased iPS- derived human hepatocytes and a variety of liver disease models. Finally, the differences in metabolic activity between the liver zones are often the cause of toxicity.[70]. A future version of the SQL-SAL will implement zonation to enable the comparison of zone 1 and zone 3 responses in Cyp expression, glutamate synthetase expression, as well as acetaminophen toxicity.

Future developments

The present SQL-SAL maintains major physiological functions for at least 28 days. The SQL-SAL can be used as a stand-alone liver model and when appropriately sized (scaled), integrated with other organ models.[71] There are a number of developments that will be implemented in the next generation SQL-SAL to further improve the physiological value of the liver model (Table 1). In particular, we will employ iPS-derived human hepatocytes with a range of normal and disease genomic backgrounds that are now being fully characterized, employ liver specific endothelial cells to optimize the biology, employ matrix-coated plastic, transition to microfluidic devices without PDMS to optimize the use with hydrophobic drugs and biologics, and employ a range of scales and total device volumes to optimize for specific applications. In addition, the SQL-SAL will be used in conjunction with a database that can not only manage, analyze, and model data, but can also access published bioassay, chemical, pre-clinical and clinical findings from public and private databases to enable predictive modeling of human hepatotoxicity risk and various models of disease progression.

A particularly valuable contribution of MPS models in the future will be the inclusion in drug discovery and development programs based on quantitative systems pharmacology (QSP).[72] QSP is an iterative process of computational methods and experimental approaches that is rooted in patient data. The development of a mathematical model of the experimental system is used to suggest new experimental steps. The inclusion of iPS-derived cells from patients with genetic and disease backgrounds in physiologically relevant experimental models will ''personalize'' the drug discovery and development process. The development of MPS models is an evolutionary process, but with revolutionary potential to change how we investigate human diseases and toxicology.[19]

Authors' contributions: All authors participated in the design, interpretation of the studies, analyses of the data and review of the manuscript. LV, NS, RB, and RDB conducted the experiments. TYS ran statistical analysis. LV, NS, AG, and DLT wrote the manuscript.

ACKNOWLEDGEMENTS

We thank Thomas Neumann at Nortis, Inc. (Seattle, Washington) for discussions on evolving microfluidic devices for next generation liver models, Edward LeCluyse (Hamner Institute), Martin Yarmush at the Massachusetts General Hospital for discussions on liver models, John Wikswo (Vanderbilt) for discussions on the engineering of organs on chips, including microclinical analyzers and Alex Soto-Gutierrez (University of Pittsburgh) for collaboration on the implementation of human iPS-derived hepatocytes. In addition, we have benefited from discussions with our collaborators involved in the integration of the liver and kidney (Jonathan Himmelfarb and Edward Kelly, University of Washington), and the gut with Mary Estes (Baylor University) and Mark Donowitz (Johns Hopkins). We also thank our collaborators at the University of Pittsburgh on a variety of liver disease models (Alan Wells, Jaideep Behari, Vinod Rustgi, Paul Monga and Ed Prochownik). We thank the University of Pittsburgh Cancer Institute (UPCI) Vector Core Facility and Dr. Robert W. Sobol for assistance with lentiviral materials. Support for the UPCI Vector Core Facility was provided by the Cancer Center Support Grant from the National Institutes of Health P30 CA047904. This project used the UPCI Chemical Biology Facility that **is** supported in part by award P30CA047904. This work was supported in part by the National Institutes of Health Common Fund and the National Center for Advancing Translational Sciences (#5UH2TR000503-02, #4UH3TR000503–03, 3UH2TR000503-02S1) and P30CA047904. Research reported in this publication was supported by the Office Of The Director, National Institutes Of Health of the National Institutes Of Health under Award Number S10OD012269. The content is solely the responsibility of the authors and does not necessarily represent the official views of the National Institutes Of Health.

REFERENCES

1. Greaves P, Williams A, Eve M. First dose of potential new medicines to humans: how animals help. *Nat Rev Drug Dis* 2004;**3**:226–36
2. Krewski D, Acosta D Jr., Andersen M, Anderson H, Bailar JC, 3rd, Boekelheide K, Brent R, Charnley G, Cheung VG, Green S Jr., Kelsey KT, Kerkvliet NI, Li AA, McCray L, Meyer O, Patterson RD, Pennie W, Scala RA, Solomon GM, Stephens M, Yager J, Zeise L. Toxicity testing in the 21st century: a vision and a strategy. *J Toxicol Environment Health Part B, Crit Rev* 2010;**13**:51–138
3. Soldatow VY, Lecluyse EL, Griffith LG, Rusyn I. models for liver toxicity testing. *Toxicol Res* 2013;**2**:23–39

4. Mayne JT, Ku WW, Kennedy SP. Informed toxicity assessment in drug discovery: systems-based toxicology. *Curr Opin Drug Discov Develop* 2006;**9**:75–83
5. Patlewicz G, Simon T, Goyak K, Phillips RD, Rowlands JC, Seidel SD, Becker RA. Use and validation of HT/HC assays to support 21st century toxicity evaluations. *Regulator Toxicol Pharmacol* 2013;**65**:259–68
6. Messner S, Agarkova I, Moritz W, Kelm JM. Multi-cell type human liver microtissues for hepatotoxicity testing. *Arch Toxicol* 2013;**87**:209–13
7. Kostadinova R, Boess F, Applegate D, Suter L, Weiser T, Singer T, Naughton B, Roth A. A long-term three dimensional liver co-culture system for improved prediction of clinically relevant drug-induced hepatotoxicity. *Toxicol Appl Pharmacol* 2013;**268**:1–16
8. Bale SS, Vernetti L, Senutovitch N, Jindal R, Hegde M, Gough A, McCarty WJ, Bakan A, Bhushan A, Shun TY, Golberg I, DeBiasio R, Usta OB, Taylor DL, Yarmush ML. In vitro platforms for evaluating liver toxicity. *Experimental biology and medicine* 2014;**239**:1180–91
9. Giuliano KA, Gough AH, Taylor DL, Vernetti LA, Johnston PA. Early safety assessment using cellular systems biology yields insights into mechanisms of action. *J Biomol Screen* 2010;**15**:783–97
10. Kepp O, Galluzzi L, Lipinski M, Yuan J, Kroemer G. Cell death assays for drug discovery. *Nat Rev Drug Discov* 2011;**10**:221–37
11. McKim JM Jr. Building a tiered approach to in vitro predictive toxicity screening: a focus on assays with in vivo relevance. *Combinat Chem High Throughput Screen* 2010;**13**:188–206
12. Vernetti L, Irwin W, Giuliano KA, Gough A, Johnston K, Taylor DL. Cellular systems biology applied to preclinical safety testing: a case study of CellCiphr^{TM} profiling. *Drug Efficacy, Safety Biol Discov: Emerg Technol Tool* 2009;**4**:53
13. Aleo MD, Luo Y, Swiss R, Bonin PD, Potter DM, Will Y. Human drug-induced liver injury severity is highly associated with dual inhibition of liver mitochondrial function and bile salt export pump. *Hepatology* 2014;**60**:1015–22
14. Will Y, Schroeter T. Deployment of in silico and in vitro safety assays in early-stage drug discovery. *Future medicinal chemistry* 2012;**4**:1211–3
15. Greene N, Aleo MD, Louise-May S, Price DA, Will Y. Using an in vitro cytotoxicity assay to aid in compound selection for in vivo safety studies. *Bioorganic Medicinal Chem Lett* 2010;**20**:5308–12
16. Lin Z, Will Y. Evaluation of drugs with specific organ toxicities in organ-specific cell lines. *Toxicol Sci: Official J Soc Toxicol* 2012;**126**:114–27
17. Xu JJ, Henstock PV, Dunn MC, Smith AR, Chabot JR, de Graaf D. Cellular imaging predictions of clinical drug-induced liver injury. *Toxicol Sci: Official J Soc Toxicol* 2008;**105**:97–105
18. Bhatia SN, Ingber DE. Microfluidic organs-on-chips. *Nat Biotechnol* 2014;**32**:760–72
19. Wikswo JP (ed.). Annual thematic issue: the biology and medicine of microphysiological systems. Annual thematic issue: the biology and medicine of microphysiological systems. *Experiment Biol Med* 2014;**239**:1061–271
20. Unger RE, Krump-Konvalinkova V, Peters K, Kirkpatrick CJ. In vitro expression of the endothelial phenotype: comparative study of primary isolated cells and cell lines, including the novel cell line HPMEC-ST1.6R. *Microvasc Res* 2002;**64**:384–97
21. Jang CH, Choi JH, Byun MS, Jue DM. Chloroquine inhibits production of TNF-alpha, IL-1beta and IL-6 from lipopolysaccharide-stimulated human monocytes/macrophages by different modes. *Rheumatology* 2006;**45**:703–10
22. Xu L, Hui AY, Albanis E, Arthur MJ, O'Byrne SM, Blaner WS, Mukherjee P, Friedman SL, Eng FJ. Human hepatic stellate cell lines, LX-1 and LX-2: new tools for analysis of hepatic fibrosis. *Gut* 2005;**54**:142–51
23. Bonner JC. Regulation of PDGF and its receptors in fibrotic diseases. *Cytokine Growth Factor Rev* 2004;**15**:255–73
24. Tourovskaia A, Fauver M, Kramer G, Simonson S, Neumann T. Tissue-engineered microenvironment systems for modeling human vasculature. *Experiment Biol Med* 2014;**239**:1264–71
25. Hegde M, Jindal R, Bhushan A, Bale SS, McCarty WJ, Golberg I, Usta OB, Yarmush ML. Dynamic interplay of flow and collagen stabilizes primary hepatocytes culture in a microfluidic platform. *Lab Chip* 2014;**14**:2033–9
26. Godoy P, Hewitt NJ, Albrecht U, Andersen ME, Ansari N, Bhattacharya S, Bode JG, Bolleyn J, Borner C, Bottger J, Braeuning A, Budinsky RA, Burkhardt B, Cameron NR, Camussi G, Cho CS, Choi YJ, Craig Rowlands J, Dahmen U, Damm G, Dirsch O, Donato MT, Dong J, Dooley S, Drasdo D, Eakins R, Ferreira KS, Fonsato V, Fraczek J, Gebhardt R, Gibson A, Glanemann M, Goldring CE, Gomez-Lechon MJ, Groothuis GM, Gustavsson L, Guyot C, Hallifax D, Hammad S, Hayward A, Haussinger D, Hellerbrand C, Hewitt P, Hoehme S, Holzhutter HG, Houston JB, Hrach J, Ito K, Jaeschke H, Keitel V, Kelm JM, Kevin Park B, Kordes C, Kullak-Ublick GA, LeCluyse EL, Lu P, Luebke-Wheeler J, Lutz A, Maltman DJ, Matz-Soja M, McMullen P, Merfort I, Messner S, Meyer C, Mwinyi J, Naisbitt DJ, Nussler AK, Olinga P, Pampaloni F, Pi J, Pluta L, Przyborski SA, Ramachandran A, Rogiers V, Rowe C, Schelcher C, Schmich K, Schwarz M, Singh B, Stelzer EH, Stieger B, Stober R, Sugiyama Y, Tetta C, Thasler WE, Vanhaecke T, Vinken M, Weiss TS, Widera A, Woods CG, Xu JJ, Yarborough KM, Hengstler JG. Recent advances in 2D and 3D in vitro systems using primary hepatocytes, alternative hepatocyte sources and non-parenchymal liver cells and their use in investigating mechanisms of hepatotoxicity, cell signaling and ADME. *Archive Toxicol* 2013;**87**:1315–530
27. Khetani SR, Kanchagar C, Ukairo O, Krzyzewski S, Moore A, Shi J, Aoyama S, Aleo M, Will Y. Use of micropatterned cocultures to detect compounds that cause drug-induced liver injury in humans. *Toxicol Sci: Official J Soc Toxicol* 2013;**132**:107–17
28. Hynes J, Nadanaciva S, Swiss R, Carey C, Kirwan S, Will Y. A high-throughput dual parameter assay for assessing drug-induced mitochondrial dysfunction provides additional predictivity over two established mitochondrial toxicity assays. *Toxicol in vitro: an international journal published in association with BIBRA* 2013;**27**:560–9
29. Nadanaciva S, Aleo MD, Strock CJ, Stedman DB, Wang H, Will Y. Toxicity assessments of nonsteroidal anti-inflammatory drugs in isolated mitochondria, rat hepatocytes, and zebrafish show good concordance across chemical classes. *Toxicol Appl Pharmacol* 2013;**272**:272–80
30. Ebrahimkhani MR, Neiman JA, Raredon MS, Hughes DJ, Griffith LG. Bioreactor technologies to support liver function in vitro. *Adv Drug Deliver Rev* 2014;**69–70**:132–57
31. Xia L, Ng S, Han R, Tuo X, Xiao G, Leo HL, Cheng T, Yu H. Laminar-flow immediate-overlay hepatocyte sandwich perfusion system for drug hepatotoxicity testing. *Biomaterials* 2009;**30**:5927–36
32. Taguchi K, Matsushita M, Takahashi M, Uchino J. Development of a bioartificial liver with sandwiched-cultured hepatocytes between two collagen gel layers. *Artificial Organ* 1996;**20**:178–85
33. Langsch A, Giri S, Acikgoz A, Jasmund I, Frericks B, Bader A. Interspecies difference in liver-specific functions and biotransformation of testosterone of primary rat, porcine and human hepatocyte in an organotypical sandwich culture. *Toxicol Lett* 2009;**188**:173–9
34. Yasar U, Eliasson E, Forslund-Bergengren C, Tybring G, Gadd M, Sjoqvist F, Dahl ML. The role of CYP2C9 genotype in the metabolism of diclofenac in vivo and in vitro. *Eur J Clin Pharmacol* 2001;**57**:729–35
35. Grant MH, Burke MD, Hawksworth GM, Duthie SJ, Engeset J, Petrie JC. Human adult hepatocytes in primary monolayer culture. Maintenance of mixed function oxidase and conjugation pathways of drug metabolism. *Biochem Pharmacol* 1987;**36**:2311–6
36. Cawood ML, Field HP, Ford CG, Gillingwater S, Kicman A, Cowan D, Barth JH. Testosterone measurement by isotope-dilution liquid chromatography-tandem mass spectrometry: validation of a method for routine clinical practice. *Clin Chem* 2005;**51**:1472–9
37. Bapiro TE, Andersson TB, Otter C, Hasler JA, Masimirembwa CM. Cytochrome P450 1A1/2 induction by antiparasitic drugs: dose-dependent increase in ethoxyresorufin O-deethylase activity and mRNA caused by quinine, primaquine and albendazole in HepG2 cells. *Eur J Clin Pharmacol* 2002;**58**:537–42
38. Chang TK, Waxman DJ. Enzymatic analysis of cDNA-expressed human CYP1A1, CYP1A2, and CYP1B1 with 7-ethoxyresorufin as substrate. *Meth Mol Biol* 2006;**320**:85–90
39. Wang JD, Douville NJ, Takayama S, ElSayed M. Quantitative analysis of molecular absorption into PDMS microfluidic channels. *Ann Biomed Eng* 2012;**40**:1862–73
40. Grund N, Maier P, Giordano FA, Appelt JU, Zucknick M, Li L, Wenz F, Zeller WJ, Fruehauf S, Allgayer H, Laufs S. Analysis of self-inactivating

lentiviral vector integration sites and flanking gene expression in human peripheral blood progenitor cells after alkylator chemotherapy. *Human Gene Ther* 2010;**21**:943–56
41. Kang W, Marasco WA, Tong HI, Byron M, Wu C, Shi Y, Sun S, Sun Y, Lu Y. Anti-tat hutat2:Fc mediated protection against tat-induced neurotoxicity and HIV-1 replication in human monocyte-derived macrophages. *J Neuroinflammat* 2014;**11**:195
42. Matrai J, Chuah MK, VandenDriessche T. Recent advances in lentiviral vector development and applications. *Mol Ther: J Am Soc Gene Ther* 2010;**18**:477–90
43. Crispo M, Vilarino M, dos Santos-Neto PC, Nunez-Olivera R, Cuadro F, Barrera N, Mulet AP, Nguyen TH, Anegon I, Menchaca A. Embryo development, fetal growth and postnatal phenotype of eGFP lambs generated by lentiviral transgenesis. *Transgenic Res* 2015;**24**:31–41
44. Shaw PJ, Hopfensperger MJ, Ganey PE, Roth RA. Lipopolysaccharide and trovafloxacin coexposure in mice causes idiosyncrasy-like liver injury dependent on tumor necrosis factor-alpha. *Toxicol Sci* 2007;**100**:259–66
45. Ganey PE, Luyendyk JP, Maddox JF, Roth RA. Adverse hepatic drug reactions: inflammatory episodes as consequence and contributor. *Chemico-Biol Interact* 2004;**150**:35–51
46. Lee KS, Lee SJ, Park HJ, Chung JP, Han KH, Chon CY, Lee SI, Moon YM. Oxidative stress effect on the activation of hepatic stellate cells. *Yonsei Med J* 2001;**42**:1–8
47. Washington K, Wright K, Shyr Y, Hunter EB, Olson S, Raiford DS. Hepatic stellate cell activation in nonalcoholic steatohepatitis and fatty liver. *Human Pathol* 2000;**31**:822–8
48. Schwartz RE, Trehan K, Andrus L, Sheahan TP, Ploss A, Duncan SA, Rice CM, Bhatia SN. Modeling hepatitis C virus infection using human induced pluripotent stem cells. *Proc Natl Acad Sci USA* 2012;**109**:2544–8
49. Fontana RJ, Seeff LB, Andrade RJ, Bjornsson E, Day CP, Serrano J, Hoofnagle JH. Standardization of nomenclature and causality assessment in drug-induced liver injury: summary of a clinical research workshop. *Hepatology* 2010;**52**:730–42
50. Ostapowicz G, Fontana RJ, Schiodt FV, Larson A, Davern TJ, Han SH, McCashland TM, Shakil AO, Hay JE, Hynan L, Crippin JS, Blei AT, Samuel G, Reisch J, Lee WM Group USALFS. Results of a prospective study of acute liver failure at 17 tertiary care centers in the United States. *Ann Intern Med* 2002;**137**:947–54
51. Fontana RJ. Pathogenesis of idiosyncratic drug-induced liver injury and clinical perspectives. *Gastroenterology* 2014;**146**:914–28
52. Mathur A, Loskill P, Hong S, Lee J, Marcus SG, Dumont L, Conklin BR, Willenbring H, Lee LP, Healy KE. Human induced pluripotent stem cell-based microphysiological tissue models of myocardium and liver for drug development. *Stem Cell Res Ther* 2013;**4**:S14
53. Vunjak-Novakovic G, Bhatia S, Chen C, Hirschi K. HeLiVa platform: integrated heart-liver-vascular systems for drug testing in human health and disease. *Stem Cell Res Ther* 2013;**4**:S8
54. Bhushan A, Senutovitch N, Bale SS, McCarty WJ, Hegde M, Jindal R, Golberg I, Usta OB, Yarmush ML, Vernetti L. Towards a three-dimensional microfluidic liver platform for predicting drug efficacy and toxicity in humans. *Stem Cell Res Ther* 2013;**4**:1–6
55. Clark AM, Wheeler SE, Taylor DP, Pillai VC, Young CL, Prantil-Baun R, Nguyen T, Stolz DB, Borenstein JT, Lauffenburger DA, Venkataramanan R, Griffith LG, Wells A. A microphysiological system model of therapy for liver micrometastases. *Exp Biol Med (Maywood)* 2014
56. Judson R, Houck K, Martin M, Knudsen T, Thomas RS, Sipes N, Shah I, Wambaugh J, Crofton K. In vitro and modelling approaches to risk assessment from the U.S. Environmental Protection Agency ToxCast programme. *Basic Clini Pharmacol Toxicol* 2014;**115**:69–76
57. Griffith LG, Wells A, Stolz DB. Engineering liver. *Hepatology* 2014;**60**:1426–34
58. Mammoto T, Mammoto A, Ingber DE. Mechanobiology and developmental control. *Ann Rev Cell Develop Biol* 2013;**29**:27–61
59. Knudsen TB, Keller DA, Sander M, Carney EW, Doerrer NG, Eaton DL, Fitzpatrick SC, Hastings KL, Mendrick DL, Tice RR, Watkins PB, Whelan M. FutureTox II: in vitro data and in silico models for predictive toxicology. *Toxicol Sci: Official J Soc Toxicol* 2015;**143**:256–67
60. Adams DH, Ju C, Ramaiah SK, Uetrecht J, Jaeschke H. Mechanisms of immune-mediated liver injury. *Toxicol Sci: Official J Soc Toxicol* 2010;**115**:307–21
61. Carter-Kent C, Zein NN, Feldstein AE. Cytokines in the pathogenesis of fatty liver and disease progression to steatohepatitis: implications for treatment. *Am J Gastroenterol* 2008;**103**:1036–42
62. Friedman SL. Hepatic stellate cells: protean, multifunctional, and enigmatic cells of the liver. *Physiol Rev* 2008;**88**:125–72
63. Carotti S, Morini S, Corradini SG, Burza MA, Molinaro A, Carpino G, Merli M, De Santis A, Muda AO, Rossi M, Attili AF, Gaudio E. Glial fibrillary acidic protein as an early marker of hepatic stellate cell activation in chronic and posttransplant recurrent hepatitis C. *Liver Transplant: official publication of the American Association for the Study of Liver Diseases and the International Liver Transplantation Society* 2008;**14**:806–14
64. Carpino G, Franchitto A, Morini S, Corradini SG, Merli M, Gaudio E. Activated hepatic stellate cells in liver cirrhosis. A morphologic and morphometrical study. *Italian J Anatomy Embryol = Archivio italiano di anatomia ed embriologia* 2004;**109**:225–38
65. Carpino G, Morini S, Ginanni Corradini S, Franchitto A, Merli M, Siciliano M, Gentili F, Onetti Muda A, Berloco P, Rossi M, Attili AF, Gaudio E. Alpha-SMA expression in hepatic stellate cells and quantitative analysis of hepatic fibrosis in cirrhosis and in recurrent chronic hepatitis after liver transplantation. *Digest Liver Disease: official journal of the Italian Society of Gastroenterology and the Italian Association for the Study of the Liver* 2005;**37**:349–56
66. Salliot C, van der Heijde D. Long-term safety of methotrexate monotherapy in patients with rheumatoid arthritis: a systematic literature research. *Ann Rheumat Dis* 2009;**68**:1100–4
67. Kaplowitz N, DeLeve LD. *Drug-induced liver disease*. New York, USA: Academic Press, 2013
68. Taura K, Miura K, Iwaisako K, Osterreicher CH, Kodama Y, Penz-Osterreicher M, Brenner DA. Hepatocytes do not undergo epithelial-mesenchymal transition in liver fibrosis in mice. *Hepatology* 2010;**51**:1027–36
69. Wen SL, Gao JH, Yang WJ, Lu YY, Tong H, Huang ZY, Liu ZX, Tang CW. Celecoxib attenuates hepatic cirrhosis through inhibition of epithelial-to-mesenchymal transition of hepatocytes. *J Gastroenterol Hepatol* 2014;**29**:1932–42
70. Senutovitch N, Vernetti L, Boltz R, DeBiasio R, Gough A, Taylor DL. Fluorescent protein biosensors applied to microphysiological systems. *Exp Biol Med (Maywood)* 2015;**240**:795–808
71. Allen JW, Khetani SR, Bhatia SN. In vitro zonation and toxicity in a hepatocyte bioreactor. *Toxicol Sci: Official J Society Toxicol* 2005;**84**:110–9
72. Wikswo JP, Curtis EL, Eagleton ZE, Evans BC, Kole A, Hofmeister LH, Matloff WJ. Scaling and systems biology for integrating multiple organs-on-a-chip. *Lab Chip* 2013;**13**:3496–511
73. Iyengar R, Zhao S, Chung SW, Mager DE, Gallo JM. Merging systems biology with pharmacodynamics. *Sci Translat Med* 2012;**4**:126ps7
74. Sase S, Takahashi H, Shigefuku R, Ikeda H, Kobayashi M, Matsumoto N, Suzuki M. Measurement of blood flow and xenon solubility coefficient in the human liver by xenon-enhanced computed tomography. *Med Phys* 2012;**39**:7553–9
75. Yamazaki H, Shimada T. Progesterone and testosterone hydroxylation by cytochromes P450 2C19, 2C9, and 3A4 in human liver microsomes. *Archive Biochem Biophys* 1997;**346**:161–9
76. Bort R, Mace K, Boobis A, Gomez-Lechon MJ, Pfeifer A, Castell J. Hepatic metabolism of diclofenac: role of human CYP in the minor oxidative pathways. *Biochem Pharmacol* 1999;**58**:787–96
77. Tang W, Stearns RA, Wang RW, Chiu SH, Baillie TA. Roles of human hepatic cytochrome P450s 2C9 and 3A4 in the metabolic activation of diclofenac. *Chem Res Toxicol* 1999;**12**:192–9
78. Tang JB, Goellner EM, Wang XH, Trivedi RNSt, Croix CM, Jelezcova E, Svilar D, Brown AR, Sobol RW. Bioenergetic metabolites regulate base excision repair-dependent cell death in response to DNA damage. *Mol Cancer Res: MCR* 2010;**8**:67–79

(Received December 21, 2014, Accepted May 5, 2015)